ORIGINAL ARTICLE

Cellular uptake on N- and C-termini conjugated FITC of Rath cell penetrating peptides and its consequences for gene-expression profiling in U-937 human macrophages and HeLa cervical cancer cells

Jung-hua Steven Kuo and Chia-Wei Lin

Department of Pharmacy, Chia Nan University of Pharmacy and Science, Jen-Te, Tainan, Taiwan

Abstract

Rath peptide has been introduced as a delivery vector that transports various membrane-impermeable cargoes in a non-covalent fashion. In this paper, we present a study on Rath peptide conjugated with fluorescein-5-isothiocynate (FITC) differing in its N- and C-termini. We conducted cellular toxicity and uptake experiments in U-937 and HeLa cells to analyze biocompatibility profiles and translocation efficiencies of Rath peptide with FITC serving as both a cargo and a fluorescent marker. We found that the conjugation of FITC on Rath peptide at N-terminus (FITC-Rath) led to more rapid cellular uptake in U-937 cells and significantly higher cellular uptake in HeLa cells than that which occurred at C-terminus. From DNA microarray analysis, FITC-Rath induced gene expression changes in both U-937 and HeLa cells. Five overlapping regulated genes were identified, and this overlap indicated that FITC-Rath displayed some degree of generality regarding gene responses in the two cell lines used. A real-time quantitative reverse transcriptase-polymerase chain reaction was used to confirm which regulated genes were affected by FITC-Rath. Cell communication, signal transduction, cell surface receptor signaling pathway, signal transducer activity and cellular process, were identified as overlapping biological themes. These data provide useful information on molecular mechanisms for using Rath-based delivery systems.

Introduction

Rath peptide, one type of cell penetrating peptide (CPP), has been introduced as a delivery vector that transports various membrane-impermeable cargoes in a non-covalent fashion [1]. Rath peptide is derived from the C-terminus of VP5 protein domain of the infectious bursal disease virus (IBDV) found in poultry and contains four non-polar tryptophan residues that create self-assembling properties [2]. The VP5 protein of IBDV, encoded from the smallest open reading frame of segment A sequences of double-stranded RNA genome, is a highly basic, conserved and cysteine-rich class II membrane protein with cytoplasmic N-terminus and an extracellular C-terminal domain [3–5]. It has been shown that VP5 is non-essential for IBDV replication and is involved in regulating the release of intracellular IBDV virions by accumulation of itself in the host cell membrane [3,4]. Rath peptide self-aggregates to form 10–60 nm particles and has a dominant β-structure devoid of any α-helical structure [1]. Also, Rath peptide delivers cargoes into cells independent of temperature, suggesting an endocytosis-independent pathway [1]. Furthermore, Rath peptide might form Trp-cage, which can protect DNA cargo from enzymatic degradation [1]. Despite strong potential in the applications of intracellular delivery, a more complete picture of Rath peptide still needs to be developed. In this study, we investigate the characterization of Rath peptide in two cell systems. We present a study with Rath peptide conjugated with fluorescein-5-isothiocynate (FITC) differing in its N- and C-termini. We conduct cellular toxicity and uptake experiments in U-937 human macrophages and HeLa cervical cancer cells to analyze biocompatibility profiles and translocation efficiencies of Rath peptide with FITC serving as both a cargo and a fluorescent marker. Under biocompatible doses, we found that the conjugation of FITC on Rath peptide at N-terminus (FITC-Rath) led to more rapid cellular uptake in U-937 cells and significantly higher cellular uptake in HeLa cells than that which occurred at C-terminus. To further understand the precise molecular mechanism in cells after the uptake of FITC-Rath, we evaluated the alteration of whole genomic responses in U-937 macrophages and HeLa cells that had been treated with FITC-Rath by high-density microarray analysis. Since the non-specific uptake of CPPs to cells is already well-known, we attempted to observe if there is any generality in gene responses in the two cell lines used. Understanding the influences and consequences of FITC-Rath-induced gene changes should help us design and develop efficient and safe delivery systems into target cells.

Address for correspondence: Jung-hua Steven Kuo, Department of Pharmacy, Chia Nan University of Pharmacy and Science, 60 Erh-Jen Road, Sec. 1, Jen-Te, Tainan 717, Taiwan. Tel: 886-6-266-4911; ext. 2104. Fax: 886-6-266-6411. E-mail: kuojunghua@yahoo.com.tw

Materials and methods

Peptide synthesis

The Rath peptide (TPWWRLWTKWHHKRRDLPRKPEGC) and fluorescein-labeled Rath at N- and C-termini (FITC-TPW WRLWTKWHHKRRDLPRKPEGC (FITC-Rath); TPWWRL WTKWHHKRRDLPRKPEGCK-FITC (Rath-FITC)) used in this study were purchased from Genemed Synthesis (San Antonio, TX). They were prepared using solid phase peptide synthesis. The quality of the peptides was ascertained using reverse-phase high performance liquid chromatography (HPLC) and time-of-flight mass spectrometry (TOFMS). The purity of the Rath, FITC-Rath and Rath-FITC used was 97.30%, 95.39% and 95.96%; respectively. Electrospray ionization mass spectrometry (ESI-MS) was used to determine the fidelity of the synthesized peptides as follows: 3170.60 for Rath, 3673.28 for FITC-Rath and 3688.30 for Rath-FITC, respectively.

Cell culture

A human macrophage-like U-937 large-cell lymphoma cell line and a human cervical cancer cell line (HeLa) (ATCC CCL-2; American Type Culture Collection, Manassas, VA) were maintained in RPMI 1640 medium (Invitrogen Corp., Carlsbad, CA) and in a DMEM medium (Invitrogen), respectively. These cells were supplemented with 10% heat-inactivated fetal bovine serum (FBS; Gibco BRL, Life Technologies, Grand Island, NY) and 100 U/mL penicillin/100 μg/mL streptomycin (Sigma-Aldrich, St Louis, MO) in a humidified atmosphere of 5% CO_2 at 37 °C.

Cytotoxicity assay

The activity of dehydrogenases (an indicator of cell viability) in the cells (treated or untreated with peptides) was simultaneously assessed. Negative control cells contained no peptides. Cells were seeded in 96-well plates at 10 000 cells/well, which were then incubated overnight at 37 °C in an atmosphere containing 5% CO_2. Various concentrations of peptides were added to the experimental cells, which were then incubated for various time periods. Ten microliters of a cell-counting kit (Cell Counting Kit-8; Dojindo Laboratories, Japan) solution, which contains a tetrazolium salt that produces a highly water-soluble formazan dye when biochemically reduced in the presence of an electron carrier (1-methoxy PMS) were added to 100 μL of culture medium and incubated for 4 h. The absorbance at 450 nm was obtained using an ELISA reader with a reference wavelength of 595 nm. Results are reported as the cell-viability percentage (average optical density (OD)/average negative-control OD) ± standard deviation (SD).

Cellular uptake of FITC-Rath and Rath-FITC

The cells $(1 \times 10^6/\text{mL})$ were treated with various doses of peptides for the entire incubation period, as indicated. After the cells had been incubated, peptides were removed from the medium and washed with PBS for further analysis. The cells were then incubated with trypsin (1 mg/mL) (Sigma-Aldrich) for 15 min at 37 °C to remove membrane-bound peptides. The cells were washed once more with PBS, and then cell fluorescence was measured using flow cytometry (FACScan;

Becton, Dickinson and Company, Franklin Lakes, NJ). A 15-mM air-cooled argon-ion laser was used to excite fluorescent FITC at 488 nm, and the emitted fluorescence was measured using a 530/30-nm band-pass optical filter. Samples were run using 10^4 cells per test sample. Data were analyzed using the CELLQUEST programs (Becton, Dickinson and Company, Franklin Lakes, NJ). Negative control cells contained no peptides.

RNA purification and microarray analysis

Under the same incubation conditions as the cellular uptake assay, a reagent (Trizol; Invitrogen) was used to extract total RNA from both untreated and FITC-Rath-treated U-937/ HeLa cells. The RNA was then purified using a kit (RNeasy Mini Kit; Qiagen GmbH, Hilden, Germany). The purified RNA was quantified at an OD of 260 nm using a spectrophotometer (ND-1000; Nanodrop Technologies, Wilmington, DE) and qualitatively analyzed using a bioanalyzer (2100; Agilent Technologies, Santa Clara, CA). Microarray experiments were done following the manufacturer's protocols. In short, 0.5 μg of total RNA was amplified using a kit (Fluorescent Linear Amplification Kit; Agilent) and labeled with Cy3-CTP or Cy5-CTP (CyDye; PerkinElmer, Waltham, MA) during *in vitro* transcription. RNA from cells treated with FITC-Rath was labeled using Cy5, and RNA from untreated cells was labeled using Cy3. Cy-labeled cRNA (0.825 μg) was fragmented to an average size of about 50–100 nucleotides (nt) using incubation with a fragmentation buffer (Agilent) at 60 °C for 30 min. The fragmented labeled cRNA was then pooled and hybridized to an oligo microarray kit (Whole Human Genome Microarray [4×44 K] kit; Agilent) at 60 °C for 17 h. After they had been washed and dried with a nitrogen gun, the microarrays were scanned (microarray scanner; Agilent) at 535 nm for Cy3 and at 625 nm for Cy5. Scanned images were analyzed (Feature Extraction Software 9.5.3; Agilent) using an image analysis and normalization software to quantify signal and background intensity for each feature. The data were substantially normalized using the rank-consistency-filtering locally weighted scatterplot smoothing (LOWESS) method. Genes in which expression increased ≥2 times or decreased ≤0.5 times and that also had a *p* value <0.05 were considered to be induced. The Kyoto Encyclopedia of Genes and Genomes (KEGG) database was performed to search pathway maps for biological interpretation of high-level systemic functions. Expression analysis systematic explorer (EASE) analysis was used to identify biological themes of significant genes [6].

Real-time quantitative RT-PCR

The same RNA isolated for the microarrays was used for RT-QPCR. To prepare a cDNA pool from each RNA sample, total RNA (5 μg) was reverse-transcribed using reverse transcriptase (Moloney murine leukemia virus [M-MLV]; Promega, Madison, WI). The resulting samples were diluted 40 times by volume with nuclease-free water. Each cDNA pool was stored at −20 °C until it was subjected to an additional real-time qPCR with specific oligonucleotide primer pairs from the Roche Universal Probe Library (Roche Diagnostics, Roche Applied Science, Indianapolis, IN). Human TATA

box binding protein (TBP) was used as the reference gene. The specificity of each primer pair was tested using rat common reference RNA (Stratagene, La Jolla, CA) as a template for RT-QPCR, after which a DNA 500 chip run on the bioanalyzer was used to check the size of the PCR product. Primer pairs that yielded the predicted product at the predicted size, and no other primary or secondary products, were chosen for RT-QPCR reaction (LightCycler Instrument 1.5 using LightCycler FastStart DNA MasterPLUS SYBR Green I kit (Cat. 03 515 885 001), Roche, Castle Hill, Australia). Briefly, 10-μL reactions contained 2 μL of 5 $\times$ Master Mix, 2 μL of each 3.75-μM forward and reverse primer mixture, and 6 μL of cDNA (40:1 dilution). Each sample was run in triplicate. The RT-QPCR program was as follows: 95 °C for 10 min, 50 cycles at 95 °C for 10 s, 60 °C for 15 s and 72 °C for 10 s. At the end of the program, a melting curve analysis was conducted. For each RT-QPCR run, the data were automatically analyzed by the system and an amplification plot was generated for each cDNA sample. From each of these plots, the system automatically calculated the CP value (crossing point; the turning point corresponds to the first maximum of the second derivative curve), which we infer to be the beginning of exponential amplification. Six genes (*BIRC3*, *DOHH*, *EID3*, *GNA11*, *MAGEE1* and *PHLDB2*) were investigated using the following primer sequences: *BIRC3*: sense GCCCCACCTATTGGAAGAAG and antisense CCCAAGCATTGCTAACCAGT; *DOHH*: sense TGTCATCGCTTGTGTCTTGC and antisense TCAG GGAGTCACAGCACAAC; *EID3*: sense GGTGAGGGAAA TGATTCCAG and antisense AGCTGCCACAATGTTTTT CC; *GNA11*: sense CTCGCACCTGGTGGACTACT and anti-sense AACACGAAGCGGATGTTCTC; *MAGEE1*: sense GT GTTCCCTGACCTCCTGAA and antisense TCCATCTCCC TTCGGTTGTA; and *PHLDB2*: GGCAACCAGTAGCCAAT GTC and antisense GGGAGCAGTTAGCAGGTGTG.

Statistical analysis

Statistical analysis was done using a one-way analysis of variance (ANOVA). Significance was set at $p < 0.05$. The data from cells treated with peptides at different doses were compared with data from untreated cells at each corresponding incubation time.

Results

Cytotoxicity assay

To determine cell viability, we used a cytotoxicity assay to measure intracellular dehydrogenase activity in mitochondria. We incubated U-937 cells with various concentrations of Rath, FITC-Rath and Rath-FITC for up to 24 h of incubation (Figure 1). Cell viability was above 80% at concentrations up to 15 μM of Rath, FITC-Rath and Rath-FITC. After conjugation of FITC at N- or C-termini of Rath peptide, the concentrations above 80% cell viabilities of FITC-Rath and Rath-FITC were higher than in Rath peptides (Figure 1B and C). The same concentration profiles of cell viability were also observed for Rath-, FITC-Rath- and Rath-TITC-treated HeLa cells. For reasons of biocompatibility, the following uptake experiments were conducted with not more than 15-μM doses of FITC-Rath and Rath-FITC.
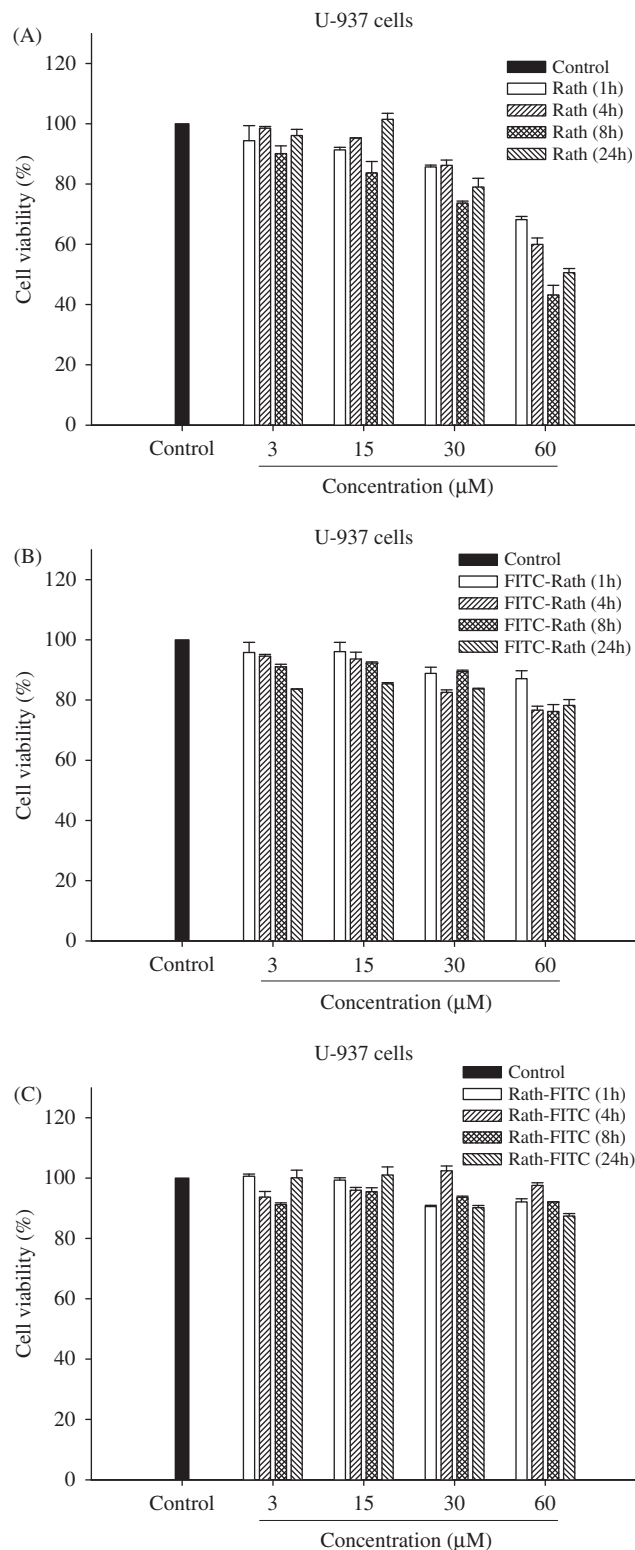

Figure 1. Cytotoxicity assays of (A) Rath, (B) FITC-Rath and (C) Rath-TITC on U-937 cells by measuring generated dehydrogenases. Negative control cells were grown without adding peptides. Data are illustrated as cell viability percentages (average OD/average negative control OD) $\pm$ standard deviation (SD) ($n = 3$).

Cellular uptake of FITC-Rath and Rath-FITC

The cellular uptake of FITC-Rath and Rath-FITC was conducted by a FACS analysis (Figure 2). After treatment of FITC-Rath and Rath-FITC, U-937 cells were incubated
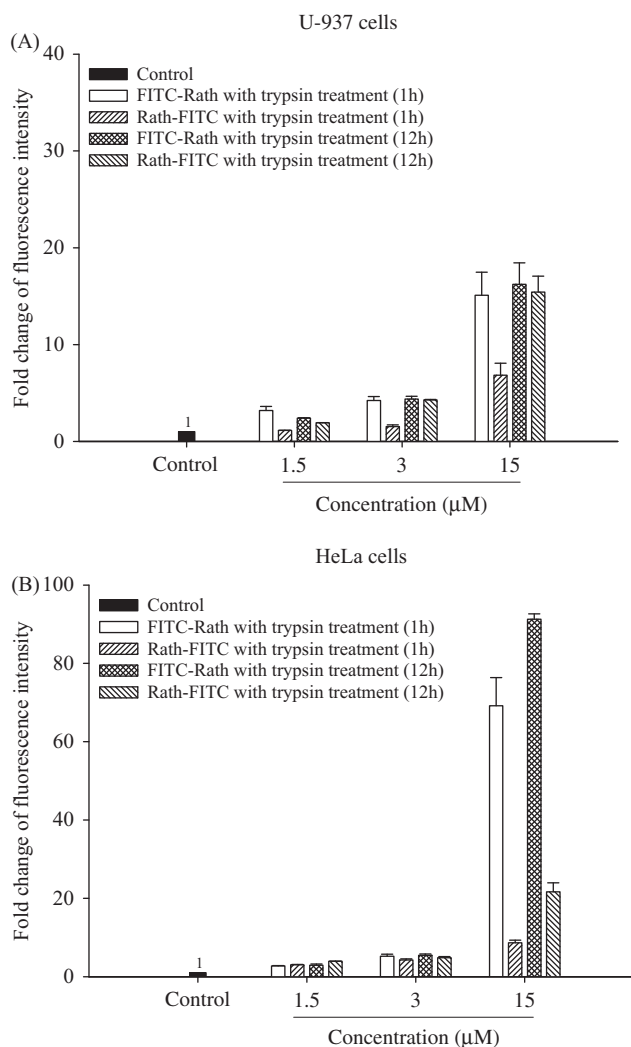
Figure 2. Flow cytometric analysis of the kinetics of FITC-Rath and Rath-FITC uptake in (A) U-937 and (B) HeLa cells. FITC fluorescence intensities in cells treated with FITC-Rath or Rath-FITC with trypsin at different doses and for different times. Control cells were grown by adding 15 mM FITC. Data are expressed as means ± standard deviations ($n = 3$).

with trypsin to remove surface-bound peptide (Figure 2A). Cells incubated with both FITC-Rath and Rath-FITC showed a significant increase in cell fluorescence at 15 μM dose after 1 h and 12 h of incubation. The fold change of fluorescence intensity of FITC-Rath was significantly higher than that of Rath-FITC at 15 μM dose after 1 h of incubation, but the cellular uptake between FITC-Rath and Rath-FITC was comparable at 15 μM dose after 12 h of incubation. This indicated that the labeling of FITC on Rath peptide at N-terminus led to more rapid cellular uptake than that which occurred at C-terminus in U-937 cells. At 15 μM dose, the cellular uptakes of FITC-Rath were also considerably higher than those found in Rath-FITC after 1 h and 12 h in HeLa cells (Figure 2B). Notably, the increase in the fold change of fluorescence intensity of FITC-Rath in HeLa cells was more pronounced than the increase in U-937 cells. Therefore, we selected the labeling of FITC with Rath peptide at N-terminus (FITC-Rath) at 15 μM dose after 12 h of incubation in U-937 and HeLa cells for microarray investigation.

Global gene expression profiles of U-937 and HeLa cells treated with FITC-Rath

To understand the non-specific effects of gene expression in different cell lines by Rath cell-penetrating peptides, global gene expression profiles were generated in 15 μM FITC-Rath-treated U937/HeLa cells after 12 h of incubation using whole-genome oligonucleotide microarrays. The criterion for differential expression of both upregulated and downregulated genes affected by FITC-Rath was an increase ≥ 2 times or a decrease ≤ 0.5 times (Tables 1 and 2). In U-937 cells, a total of 35 genes, which contained 16 upregulated genes and 19 downregulated genes, were affected by FITC-Rath (Table 1). In HeLa cells, a total of 27 genes, which included 11 upregulated genes and 16 downregulated genes, were affected by FITC-Rath (Table 2). The number of upregulated and downregulated genes in U-937 cells was slightly higher than the number observed in HeLa genes. Although there were no overlapping upregulated genes in U-937 and HeLa cells, five overlapping downregulated genes (*HKDC1*, *HSD11B2*, *C1QTNF5*, *MAGEE1* and *PADI6*) were identified. This indicated that FITC-Rath can cause some common regulated genes in both U-937 and HeLa cells. Next, all genes reported in Tables 1 and 2 were subjected to gene ontology (GO) clustering by the EASE analysis for identifying the top 10 biological themes within the gene lists (Tables 3 and 4). The overlapping categories in both U-937 and HeLa cells treated with FITC-Rath were as follows: cell communication, signal transduction, cell surface receptor signaling pathway, signal transducer activity and cellular process. These results may also indicate the common reactions of both U-937 and HeLa cells treated with FITC-Rath. After using KEGG pathway analysis, no common pathway was found for those significant genes in Tables 1 and 2.

Confirming microarray results using RT-QPCR

To compare the gene expression results obtained from the microarray analysis with the results from RT-QPCR, we tested two upregulated genes (*BIRC3* and *DOHH*, which are responsible for cell death and enzyme activity, respectively) and two downregulated genes (*GNA11* and, which are responsible for cell communication and antigen binding, respectively) in U-937 cells, and three downregulated genes (*EID3*, *MAGEE1* and *PHLDB2*, which are responsible for transcription activity, antigen binding and cell migration, respectively) in HeLa cells. The criteria for selecting genes measured using RT-QPCR were based on their diverse biological functions in the cells. The downregulated gene (*MAGEE1*) overlaps in both U-937 and HeLa cells. The RT-QPCR results were quantitatively consistent with the results from the microarray (Figure 3).

Discussion

We performed a comparative uptake analysis of the two FITC-conjugated Rath cell penetrating peptides (the N- and C-termini conjugated FITC of Rath peptides) on U-937 and HeLa cells (Figure 2). We demonstrated that the conjugation of FITC on Rath peptide at N-terminus led to more rapid cellular uptake in U-937 cells and significantly higher cellular

Table 1. Upregulated and downregulated genes in U-937 cells.

Gene name	GeneBank number	Description	Fold change
Upregulated			
CXCL10	NM_001565	Homo sapiens chemokine (C-X-C motif) ligand 10	14.28
RAD21L1	NM_001136566	Homo sapiens RAD21-like 1 (S. pombe)	2.95
KLF5	NM_001730	Homo sapiens Kruppel-like factor 5 (intestinal)	2.82
KITLG	NM_000899	Homo sapiens KIT ligand (KITLG), transcript variant b	2.78
ALOX5	NM_000698	Homo sapiens arachidonate 5-lipoxygenase (ALOX5)	2.64
SLC32A1	NM_080552	Homo sapiens solute carrier family 32 (GABA vesicular transporter), member 1	2.59
DARC	NM_002036	Homo sapiens Duffy blood group, chemokine receptor (DARC), transcript variant 2	2.56
HRASLS2	NM_017878	Homo sapiens HRAS-like suppressor 2	2.54
TRIM23	NM_001656	Homo sapiens tripartite motif-containing 23 (TRIM23), transcript variant alpha	2.44
PDE6H	NM_006205	Homo sapiens phosphodiesterase 6H, cGMP-specific, cone, gamma	2.24
TP53	NM_000546	Homo sapiens tumor protein p53 (TP53), transcript variant 1	2.19
DST	NM_001723	Homo sapiens dystonin (DST), transcript variant 1 e beta 1 subunit (AP2B1), transcript variant 1	2.18
DOHH	NM_031304	Homo sapiens deoxyhypusine hydroxylase/monooxygenase (DOHH), transcript variant 2	2.18
BAIAP2	NM_017451	Homo sapiens BAI1-associated protein 2 (BAIAP2), transcript variant 2	2.13
PPP2R2C	NM_020416	Homo sapiens protein phosphatase 2, regulatory subunit B, gamma (PPP2R2C), transcript variant 1	2.01
BIRC3	NM_001165	Homo sapiens baculoviral IAP repeat-containing 3 (BIRC3), transcript variant 1	2.00
Downregulated			
HKDC1*	NM_025130	Homo sapiens hexokinase domain containing 1	0.04
HSD11B2*	NM_000196	Homo sapiens hydroxysteroid (11-beta) dehydrogenase 2	0.14
C1QTNF5*	NM_015645	Homo sapiens C1q and tumor necrosis factor related protein 5	0.20
GNA11	NM_002067	Homo sapiens guanine nucleotide binding protein (G protein), alpha 11 (Gq class)	0.24
LBH	NM_030915	Homo sapiens limb bud and heart development homolog (mouse)	0.26
MAGEE1*	NM_020932	Homo sapiens melanoma antigen family E, 1	0.26
MED18	NM_017638	Homo sapiens mediator complex subunit 18 (MED18), transcript variant 1	0.32
EPHA8	NM_020526	Homo sapiens EPH receptor A8 (EPHA8), transcript variant 1	0.37
GRIP1	NM_021150	Homo sapiens glutamate receptor interacting protein 1 (GRIP1), transcript variant 1	0.39
LENG9	NM_198988	Homo sapiens leukocyte receptor cluster (LRC) member 9	0.40
ZNF687	NM_020832	Homo sapiens zinc finger protein 687	0.41
PADI6*	NM_207421	Homo sapiens peptidyl arginine deiminase, type VI	0.42
TNXB	NM_032470	Homo sapiens tenascin XB (TNXB), transcript variant XB-S	0.42
KIF18B	NM_001080443	Homo sapiens kinesin family member 18B	0.45
SHROOM1	NM_133456	Homo sapiens shroom family member 1	0.46
ADAMTS13	NM_139025	Homo sapiens ADAM metallopeptidase with thrombospondin type 1 motif, 13 (ADAMTS13), transcript variant 1	0.48
C15orf27	NM_152335	Homo sapiens chromosome 15 open reading frame 27	0.48
KCTD17	NM_024681	Homo sapiens potassium channel tetramerization domain containing 17	0.49
NR4A2	NM_006186	Homo sapiens nuclear receptor subfamily 4, group A, member 2	0.49

*Genes affected in both U-937 and HeLa cells.

uptake in HeLa cells than which occurred at the C-terminus. In a previous study, another amphipathic and non-covalent cell penetrating peptide Pep-1 also showed the difference in translocation efficiency between N- and C-termini end groups [7]. The authors demonstrated that the tryptophan-rich domain in Pep-1 served as the main membrane-anchoring region and that the additional higher membrane affinity of the Pep-1 termini was responsible for the increased translocation efficiencies for the various proteins. Since the same end group (FITC) in Rath peptide was used in our study, our results also demonstrated that the position of FITC may be associated with the membrane affinity of the peptide. Since the tryptophan-rich domain in Rath peptide was located in N-termini, FITC-conjugated Rath at the N-termini led to higher membrane affinity and increased cellular uptake than the FITC-conjugated Rath at the C-termini. These results were consistent with those of a previous study [7]. Also, cellular uptake of 15 μM FITC with Rath peptide into both U-937 and HeLa cells by non-covalent mixing was not observed during the flow cytometry analysis. This indicates that the ability of non-covalent transport of Rath peptide is dependent on the characteristics of cargoes.

Rath peptide has been developed from the non-structural VP5 protein of IBDV in poultry and exploited as an intracellular carrier for various membrane-impenetrable cargoes. It has been shown that VP5 plays an important role in dissemination and pathogenesis *in vivo* [8]. VP5 has been demonstrated to accumulate within the host membrane and induce cell lysis, and it has also been reported to induce apoptosis in host cells [3,9]. Although the concentration used in our study (15 μM) did not dramatically damage cell membranes, Rath peptides may act as stressors via interaction with cell membranes and lead to cellular stress responses in U-937 cells (Table 3). The immunological effects of Rath on the cells and possibly on the patient as target thus need to be further examined.

Of the seven genes confirmed by RT-QPCR, *BIRC3* has been related to anti-apoptosis in various cells [10–13]. Our results indicate that *BIRC3* upregulation is the survival signal in U-937 cells treated with FITC-Rath. *DOHH* catalyzes the activation of translation initiation factor (*eIF5A*), which is essential for cell growth [14,15]. The upregulation of *DOHH* may suggest enhanced cell proliferation in U-937 cells. *GNA11* is a member of the guanine nucleotide-binding

Table 2. Upregulated and downregulated genes in HeLa cells.

Gene name	GeneBank number	Description	Fold change
Upregulated			
COL13A1	NM_080801	Homo sapiens collagen, type XIII, alpha 1 (COL13A1), transcript variant 5	2.83
CARD9	NM_052813	Homo sapiens caspase recruitment domain family, member 9 (CARD9), transcript variant 1	2.74
GRHL3	NM_198174	Homo sapiens grainyhead-like 3 (Drosophila) (GRHL3), transcript variant 3	2.61
CXCL12	NM_199168	Homo sapiens chemokine (C-X-C motif) ligand 12 (CXCL12), transcript variant 1	2.55
MYF6	NM_002469	Homo sapiens myogenic factor 6 (herculin)	2.41
TNFRSF11A	NM_003839	Homo sapiens tumor necrosis factor receptor superfamily, member 11 a, NFKB activator	2.39
NANP	NM_152667	Homo sapiens N-acetylneuraminic acid phosphatase	2.38
SCN3B	NM_018400	Homo sapiens sodium channel, voltage-gated, type III, beta (SCN3B), transcript variant 1	2.33
GPR1	NM_005279	Homo sapiens G protein-coupled receptor 1 (GPR1), transcript variant 1	2.26
TAS2R8	NM_023918	Homo sapiens taste receptor, type 2, member 8	2.18
GRM2	NM_000839	Homo sapiens glutamate receptor, metabotropic 2 (GRM2), transcript variant 1	2.06
Downregulated			
HKDC1*	NM_025130	Homo sapiens hexokinase domain containing 1	0.02
ACTL8	NM_030812	Homo sapiens actin-like 8	0.05
C1QTNF5*	NM_015645	Homo sapiens C1q and tumor necrosis factor related protein 5	0.13
CNGB3	NM_019098	Homo sapiens cyclic nucleotide gated channel beta 3	0.15
MAGEE1*	NM_020932	Homo sapiens melanoma antigen family E, 1	0.23
FAM110B	NM_147189	Homo sapiens family with sequence similarity 110, member B	0.27
PHLDB2	NM_001134438	Homo sapiens pleckstrin homology-like domain, family B, member 2 (PHLDB2), transcript variant 1	0.29
PRRT4	NM_001174164	Homo sapiens proline-rich transmembrane protein 4 (PRRT4), transcript variant 1	0.32
EID3	NM_001008394	Homo sapiens EP300 interacting inhibitor of differentiation 3	0.38
HSD11B2*	NM_000196	Homo sapiens hydroxysteroid (11-beta) dehydrogenase 2	0.39
RNF112	NM_007148	Homo sapiens ring finger protein 112	0.41
ATM	NM_000051	Homo sapiens ataxia telangiectasia mutated	0.41
XPO5	NM_020750	Homo sapiens exportin 5	0.44
C9orf106	NM_001012715	Homo sapiens chromosome 9 open reading frame 106	0.46
DUSP9	NM_001395	Homo sapiens dual specificity phosphatase 9	0.46
PADI6*	NM_207421	Homo sapiens peptidyl arginine deiminase, type VI	0.47
PRRG2	NM_000951	Homo sapiens proline rich Gla (G-carboxyglutamic acid) 2	0.49

*Genes affected in both U-937 and HeLa cells.

Table 3. Top 10 EASE analyses for profound gene expression changes in FITC-Rath-treated U-937 cells.

System	Gene category	List hits	Population hits	EASE score
GO Biological Process	Cell communication	12	3284	2.53 E−04
GO Biological Process	Signal transduction	10	2567	1.13 E−03
GO Biological Process	Cell surface receptor signaling pathway	6	1192	1.09 E−02
GO Molecular Function	Signal transducer activity	8	2430	1.42 E−02
GO Biological Process	Organ morphogenesis	5	983	2.64 E−02
GO Biological Process	Anatomical structure morphogenesis	5	1104	3.84 E−02
GO Biological Process	Cellular process	13	6740	4.33 E−02
GO Molecular Function	Cell adhesion molecule activity	3	396	7.68 E−02
GO Biological Process	Response to stress	4	859	8.03 E−02
GO Biological Process	Cell-matrix adhesion	2	80	9.21 E−02

Table 4. Top 10 EASE analyses for profound gene expression changes in FITC-Rath-treated HeLa cells.

System	Gene category	List hits	Population hits	EASE score
GO Biological Process	Cell communication	9	3284	1.61 E−02
GO Biological Process	Cellular process	13	6740	2.01 E−02
GO Biological Process	Cell–cell signaling	4	563	2.35 E−02
GO Biological Process	G-protein coupled receptor signaling pathway	4	739	4.72 E−02
GO Biological Process	Signal transduction	7	2567	5.25 E−02
GO Molecular Function	Receptor activity	5	1574	8.47 E−02
GO Molecular Function	Signal transducer activity	6	2430	1.12 E−01
GO Molecular Function	G-protein coupled receptor activity	3	530	1.13 E−01
GO Biological Process	Cell surface receptor signaling pathway	4	1192	1.46 E−01
GO Cellular Component	Integral to membrane	7	3324	1.62 E−01

G-protein subunit family and is related to the activation of MAPK or mTOR pathways in uveal melanomas [16,17]. *GNA11* downregulation may encourage the inhibition of cell growth in HeLa cells by FITC-Rath. *MAGEE1* was discovered as a candidate cancer gene in various tumors [18,19]. Our results demonstrated that the downregulation of overlapping *MAGEE1* genes in both U-937 and HeLa cells could be associated with the anti-tumor effect of Rath peptide. *EID3*
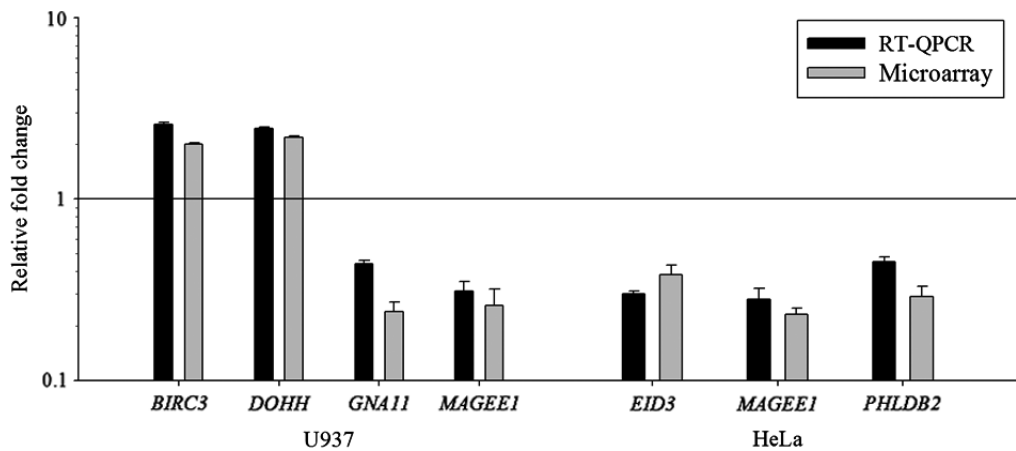
Figure 3. Confirmation of microarray results with RT-QPCR. Relative expression levels of 4 genes (*BIRC3*, *DOHH*, *GNA11* and *MAGEE1*) in U-937 cells and 3 genes (*EID3*, *MAGEE1* and *PHLDB2*) in HeLa cells incubated with FITC-Rath are shown. Data are illustrated as means ± standard deviation (SD) ($n = 3$).

inhibits nuclear receptor transcriptional activity in a tissue-specific manner, and our results showed that downregulated *EID3* may attenuate the transcriptional inhibition in HeLa cells treated with FITC-Rath [20]. *PHLDB2* has been shown to promote migration in hepatocellular carcinoma cells and our results suggest that downregulated *PHLDB2* may decrease cell migration in Hela cells [21].

The number of regulated genes in U-937 cells treated with FITC-Rath (35 genes) is compatible with the results of our previous study on FITC conjugated Tat peptide (35 genes) [22]. Four genes (*HKDC1*, *HSD11B2*, *C1QTNF5* and *MAGEE1*) were downregulated in U-937 cells by both FITC conjugated Rath and Tat. This common property may be due to virus-derived characteristics from Rath and Tat peptides. Tat has been demonstrated to be effective in downregulating tumor necrosis factor (TNF) receptors in HeLa cells and our study also demonstrated that downregulation of *C1QTNF5* by Rath peptides led to no release of TNF in either U-937 or HeLa cells [23]. However, comparing the current results with another published report, no identical genes have been found in HeLa cells treated with various CPPs including Rath [24]. This may suggest that different CPPs influence different gene-expression profiles.

There is an increased interest in the use of CPPs such as Rath for delivering biologically active cargo to cells. Furthermore, understanding the non-specific effects of these peptides on gene expression in cells is useful from a clinical point of view. The CPP Antennapedia conjugated with antisense oligonucleotide-affected specific and non-specific genes in multidrug-resistant cells [24]. After treatment of various CPPs in HeLa cells, stable expression of EGFP, changed cellular phenotype and off-target effects have been reported [25]. In this work, we give a clearer picture of the non-specific effects of CPPs on gene expression by comparing gene-expression profiles in two different cell lines. Our results suggest that overlapping downregulated genes (*HKDC1*, *HSD11B2*, *C1QTNF5*, *MAGEE1* and *PADI6*) offer candidates for further investigation of their pharmacological effects. This information may provide the target genes when applying Rath delivery.

Conclusion

We found that the conjugation of FITC on Rath peptide at N-terminus led to more rapid cellular uptake in U-937 cells and significantly higher cellular uptake in HeLa cells than that which occurred at C-terminus. From DNA microarray analysis, the conjugation of FITC on Rath peptide at N-terminus induced gene expression changes in both U-937 and HeLa cells. Five overlapping regulated genes (*HKDC1*, *HSD11B2*, *C1QTNF5*, *MAGEE1* and *PADI6*) were identified, thus indicating that FITC-Rath displayed some degree of generality regarding gene responses in the two cell lines used. Also, a real-time quantitative reverse transcriptase-polymerase chain reaction was used to confirm regulated genes affected by FITC-Rath. By EASE analysis, cell communication, signal transduction, cell surface receptor signaling pathway, signal transducer activity and cellular process, were identified as overlapping biological themes. These data provide useful information on molecular mechanisms for using Rath-based delivery systems.

Declaration of interest

The authors report no conflicts of interest. The authors alone are responsible for the content and writing of this article.

References

1. Bais MV, Kumar S, Tiwari AK, et al. Novel Rath peptide for intracellular delivery of protein and nucleic acids. Biochem Biophys Res Commun 2008;370:27–32.
2. Mundt E, Beyer J, Müller H. Identification of a novel viral protein in infectious bursal disease virus-infected cells. J Gen Virol 1995; 76:437–43.
3. Lombardo E, Maraver A, Espinosa I, et al. VP5, the nonstructural polypeptide of infectious bursal disease virus, accumulates within the host plasma membrane and induces cell lysis. Virology 2000; 277:345–57.
4. Mundt E, Köllner B, Kretzschmar D. VP5 of infectious bursal disease virus is not essential for viral replication in cell culture. J Virol 1997;71:5647–51.

5. Wu Y, Hong L, Ye J, et al. The VP5 protein of infectious bursal disease virus promotes virion release from infected cells and is not involved in cell death. Arch Virol 2009;154:1873–82.
6. Hosack DA, Dennis Jr G, Sherman BT, et al. 2003. Identifying biological themes within lists of genes with EASE. Genome Biol 2012;4:R70.
7. Weller K, Lauber S, Lerch M, et al. 2005. Biophysical and biological studies of end-group-modified derivatives of Pep-1. Biochemistry 2012;44:15799–811.
8. Yao K, Goodwin MA, Vakharia VN. Generation of a mutant infectious bursal disease virus that does not cause bursal lesions. J Virol 1998;72:2647–54.
9. Li Z, Wang Y, Xue Y, et al. Critical role for voltage-dependent anion channel 2 in infectious bursal disease virus-induced apoptosis in host cells via interaction of VP5. J Virol 2012;86:1328–38.
10. Ma O, Cai WW, Zender L, et al. MMP13, Birc2 (cIAP1), and Birc3 (cIAP2), amplified on chromosome 9, collaborate with p53 deficiency in mouse osteosarcoma progression. Cancer Res 2009; 69:2559–67.
11. Neubauer NL, Ward EC, Patel P, et al. Progesterone receptor-B induction of BIRC3 protects endometrial cancer cells from AP1-59-mediated apoptosis. Horm Cancer 2011;2:170–81.
12. Pradhan M, Baumgarten SC, Bembinster LA, Frasor J. CBP mediates NF-κB-dependent histone acetylation and estrogen receptor recruitment to an estrogen response element in the BIRC3 promoter. Mol Cell Biol 2012;32:569–75.
13. Wang Y, Tang X, Yu B, et al. Gene network revealed involvements of Birc2, Birc3 and Tnfrsf1a in anti-apoptosis of injured peripheral nerves. PLoS One 2012;7:e43436(1–10).
14. Epis MR, Giles KM, Kalinowski FC, et al. Regulation of expression of deoxyhypusine hydroxylase (DOHH), the enzyme that catalyzes the activation of eIF5A, by miR-331-3p and miR-642-5p in prostate cancer cells. J Biol Chem 2012;287:35251–9.
15. Park MH, Nishimura K, Zanelli CF, Valentini SR. Functional significance of eIF5A and its hypusine modification in eukaryotes. Amino Acids 2010;38:491–500.
16. Ho AL, Musi E, Ambrosini G, et al. Impact of combined mTOR and MEK inhibition in uveal melanoma is driven by tumor genotype. PLoS One 2012;7:e40439(1–16).
17. Khalili JS, Yu X, Wang J, et al. Combination small molecule MEK and PI3K inhibition enhances uveal melanoma cell death in a mutant GNAQ- and GNA11-dependent manner. Clin Cancer Res 2012;18:4345–55.
18. Caballero OL, Zhao Q, Rimoldi D, et al. Frequent MAGE mutations in human melanoma. PLoS One 2010;5:1–7.
19. Guillaume B, Stroobant V, Bousquet-Dubouch MP, et al. Analysis of the processing of seven human tumor antigens by intermediate proteasomes. J Immunol 2012;189:3538–47.
20. Båvner A, Matthews J, Sanyal S, et al. EID3 is a novel EID family member and an inhibitor of CBP-dependent co-activation. Nucleic Acid Res 2005;33:3561–9.
21. Lin ZY, Chuang WL. Genes responsible for the characteristics of primary cultured invasive phenotype hepatocellular carcinoma cells. Biomed Pharmacother 2012;66:454–8.
22. Lin CW, Kuo JH, Jan MS. The global gene-expression profiles of U-937 human macrophages treated with Tat peptide and Tat-FITC conjugate and Tat-FITC conjugate. J Drug Target 2012;20:515–23.
23. Fotin-Mleczek M, Welte S, Mader O, et al. Cationic cell-penetrating peptides interfere with TNF signalling by induction of TNF receptor internalization. J Cell Sci 2005;118:3339–51.
24. Fisher AA, Ye D, Sergueev DS, et al. Evaluating the specificity of antisense oligonucleotide conjugates. A DNA array analysis. J Biol Chem 2002;277:22980–4.
25. Waldeck W, Pipkorn R, Korn B, et al. Transporter molecules influence the gene expression in HeLa cells. Int J Med Sci 2009; 6:18–27.